ACS APPLIED ENERGY MATERIALS
Cite This: ACS Appl. Energy Mater. 2019, 2, 1067−1076
Article
www.acsaem.org

Collective Effect of Fe and Se To Improve the Thermoelectric Performance of Unfilled p-Type $CoSb_3$ Skutterudites

Ruchi Bhardwaj,[†,‡] Bhasker Gahtori,[*,†,‡] Kishor Kumar Johari,[†,‡] Sivaiah Bathula,[†,‡] Nagendra S. Chauhan,[†,‡] Avinash Vishwakarma,[†,‡] S. R. Dhakate,[†,‡] Sushil Auluck,[†] and Ajay Dhar[*,‡]

[†]CSIR-National Physical Laboratory, Dr. K.S. Krishnan Marg, New Delhi 110012, India
[‡]Academy of Scientific & Innovative Research (AcSIR), CSIR-NPL Campus, New Delhi 110012, India

Supporting Information

ABSTRACT: Filled skutterudites constitute an important class of efficient and stable thermoelectric materials for power generation; however, their commercialization has been hampered due to the usage of expensive rare-earth elements as "fillers" and the nonavailability of the efficient and compatible p-type counterpart. In view of this, we report a state-of-the-art thermoelectric figure of merit (ZT) in rare-earth-free p-type unfilled $CoSb_3$ skutterudite co-doped with Fe and Se, synthesized using a facile process of arc-melting and spark plasma sintering, which is both fast and scalable. The doping of Fe and Se have been chosen in accordance with the first-principles-based density functional theory (DFT) calculations which suggested that Fe leads to p-type conduction in $CoSb_3$, while Se strengthens the thermoelectric properties. The experimental results also suggest that the optimized partial substitutional doping of Fe at the Co-site and Se at the Sb-site in $CoSb_3$ leads to a favorable tuning of the electrical and thermal transport properties, which resulted in a high ZT ∼ 0.7 at 870 K in an optimized skutterudite composition of $Fe_{0.25}Co_{0.75}Sb_{2.965}Se_{0.035}$, which is the highest value reported thus far for unfilled $CoSb_3$-based p-type skutterudites. The resulting ZT of $Fe_{0.25}Co_{0.75}Sb_{2.965}Se_{0.035}$ is higher by 2 orders of magnitude than that for its pristine counterpart. In addition, the theoretically estimated transport properties of pristine and doped $CoSb_3$, calculated employing the density functional theory (DFT) and Boltzmann transport equations, were found to be in good qualitative agreement with those measured experimentally.

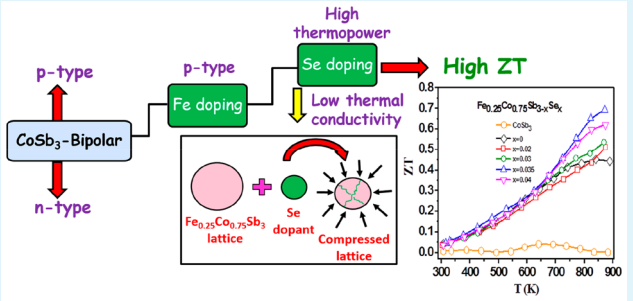

KEYWORDS: *thermoelectric, $CoSb_3$, skutterudites, figure of merit, density functional theory, band structure, transport properties*

INTRODUCTION

Thermoelectric (TE) technology is a convenient means for the generation of clean energy as it enables solid-state interconversion of heat and electricity, based on the Seebeck effect. Among the various existing green energy generation technologies, power generation using thermoelectric technology offers high reliability with the advantages of high power density, wide scalability and motionless operability.[1] The conversion efficiency of a typical thermoelectric material is quantified in terms of its dimensionless figure of merit, ZT

$$ZT = S^2\sigma T/\kappa$$

where S, σ, T, and κ are the Seebeck coefficient, electrical conductivity, absolute temperature, and thermal conductivity, respectively. Thus, the performance of a TE device is strongly influenced by the thermal and electronic transport properties of the materials used in the device fabrication. Currently, the research efforts are aimed toward enhancing the ZT of the TE materials for achieving higher thermoelectric conversion efficiency and simultaneously reducing the material and processing costs, so that this technology can compete with other existing sources of clean energy.

Several TE materials, such as tellurides, selenides, half-Heuslers, and other multi-elemental alloys, including LAST, TAGS, etc.,[2−8] have been explored for harnessing the waste-heat in the mid-temperature regime. However, the majority of these TE materials, despite possessing a high ZT in the mid-temperature range, are either unstable at the operating temperature or consist of elements that are toxic or lack a compatible n/p-type counterpart, required for efficient thermoelectric power generation. In this context, skutterudites are promising TE materials owing to their high mobility and good Seebeck coefficient[9] along with high thermal stability and relative abundance of their constituent elements.[10] Its crystal structure was identified and explained by Oftedal:[11] it has a cubic structure, and there are 32 atoms and two voids in each unit cell, with eight cubes of Co occupying the 8c sites (1/4, 1/

Received: September 25, 2018
Accepted: January 8, 2019
Published: January 8, 2019

DOI: 10.1021/acsaem.8b01609
ACS Appl. Energy Mater. 2019, 2, 1067−1076

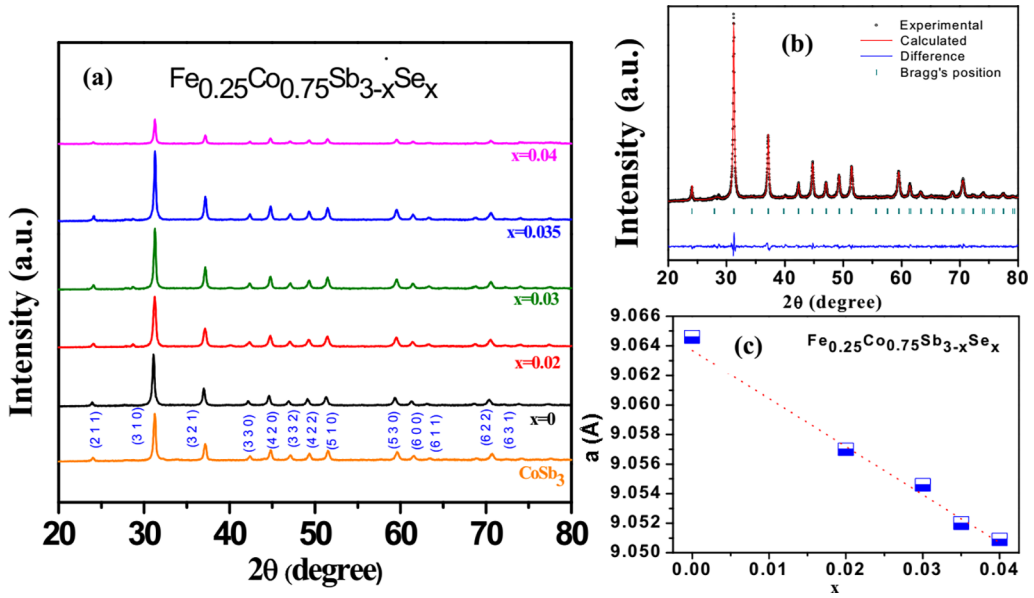

Figure 1. (a) X-ray diffraction pattern of $CoSb_3$ and $Fe_{0.25}Co_{0.75}Sb_{3-x}Se_x$ samples, (b) Rietveld refined XRD pattern, and (c) variation of lattice parameter with respect to Se doping concentration.

4, 1/4), out of which six are filled with atoms of Sb at 24g sites (0, *y*, *z*) and two voids at 2a site (0, 0, 0) and (1/2, 1/2, 1/2). These voids can be filled by atoms with smaller atomic radii. It has been well-established that there are two main conditions that must be obeyed for a filler element to enter the cage structure of the skutterudites. First, the filler element must have size consistent with the host void in the skutterudite cage structure, and second, the difference in the electronegativity has to be >0.8.[12] Thus, on the basis of their physico-chemical properties, only alkaline earths and rare earths can be considered as the main skutterudite filler elements.[10]

However, most of the conventional skutterudites possessing high ZT contain expensive rare-earth elements as "fillers", and achievement of high ZT requires multifilling of guest atoms[13−15] which induces more complexity in the synthesis. Also, it can only be synthesized as n-type TE materials by using the filling approach only,[10] which remains a major deterrent for their application for thermoelectric power generation.

Pristine binary skutterudite $CoSb_3$ behaves as a narrow band gap semiconductor, which generally exhibits bipolar conduction,[16−18] which can be favorably tuned to synthesize both n- and p-type TE materials by optimal doping. The highest reported ZT for pristine $CoSb_3$ synthesized through nanostructuring and hot pressed compaction is 0.17 at 610 K,[10,19] which is quite low due to its unoptimized carrier concentration; however, different approaches have been reported to enhance its ZT, which include doping, nanostructuring, and more recently employing a composite approach.[19−24] A ZT ∼ 0.2 at 700 K was reported in Fe doped p-type $CoSb_3$ prepared through encapsulated induction melting,[22] and the nanostructured Fe doped $CoSb_3$ synthesized by a chemical route resulted in a ZT ∼ 0.25 at 800 K.[20] Further, an enhanced ZT ∼ 0.53 at 823 K was reported by partial substitution of Fe on the Co-site in $CoSb_3$, using a microwave assisted synthesis.[25] Moreover, the co-substitutions of Mn and Sn in $CoSb_3$ yielded a ZT ∼ 0.54 at 723 K,[26] which was the highest reported thus far in p-type doped-$CoSb_3$ unfilled skutterudites, although much higher values have been reported for their n-type counterparts.[10] Feng et al.[24] have recently introduced graphene into the $CoSb_3$ matrix via a nanocomposite approach and realized an enhanced ZT ∼ 0.61 at 800 K.

In the present study, we explore the possibility of enhancing the thermoelectric performance of the unfilled $CoSb_3$-based skutterudites by employing the co-doping approach, and we report a record ZT ∼ 0.7 at 870 K in an optimized composition of $Fe_{0.25}Co_{0.75}Sb_{2.965}Se_{0.035}$, which is a rare-earth-free $CoSb_3$-based p-type TE material, synthesized using arc-melting followed by spark plasma sintering at optimized processing parameters. The experimental results suggest that the optimized partial substitutional doping of Fe at the Co-site and Se at the Sb-site in $CoSb_3$ results in a favorable tuning of the electrical and thermal transport properties leading to an enhanced ZT, which is nearly 4 times that reported earlier for its pristine counterpart.[19] On the basis of the reported studies, as the maximum ZT in doped $CoSb_3$ has been achieved for Fe doping concentration 20−30%,[20,22,27] accordingly we have fixed the Fe doping concentration at the Co-site at ∼25% and then the TE properties have been studied for different compositions by varying the Se doping concentration. In $CoSb_3$, while the Fe substitution on the Co-site results in a p-type conduction, the Se doping on the Sb-site leads to favorable tuning of the carrier concentration, resulting in enhanced electrical transport properties. These results are also supported by the theoretically derived electrical transport properties, calculated using first-principles DFT-based band structure calculations and Boltzmann transport theory.

EXPERIMENTAL DETAILS

Pristine and doped $CoSb_3$ samples were synthesized employing arc-melting (MAM-I) of the constituent elements in proper stoichiometric compositions, which was repeated several times to ensure chemical homogeneity in the arc-melted ingots. The arc-melted ingot was then pulverized, and the resulting powders were spark plasma sintered (Dr. Sinter, 725) at 600 °C with a heating rate of 200 °C/min, under compressive loading of 60 MPa using a 12.7 mm high-density SPS-grade graphite die/punches. The phase identification was carried out using X-ray diffraction (XRD, Rigaku), and the scanning electron microscope (SEM) was used to study the morphology of the synthesized samples. The quantitative elemental composition was

DOI: 10.1021/acsaem.8b01609
ACS Appl. Energy Mater. 2019, 2, 1067−1076

Table 1. Rietveld Refined Crystallographic Parameters for Pristine and Doped $CoSb_3$ Samples

	$a = b = c$ (Å)	$\alpha = \beta = \gamma$	cell volume	χ^2	R_F	R_{Bragg}
$CoSb_3$	9.0660	90°	745.15	5.97	2.37	2.74
$Fe_{0.25}Co_{0.75}Sb_3$	9.0646	90°	744.81	1.93	1.12	1.37
$Fe_{0.25}Co_{0.75}Sb_{2.98}Se_{0.02}$	9.057	90°	742.94	3.33	1.36	1.72
$Fe_{0.25}Co_{0.75}Sb_{2.97}Se_{0.03}$	9.0546	90°	742.35	1.83	0.906	1.17
$Fe_{0.25}Co_{0.75}Sb_{2.965}Se_{0.035}$	9.052	90°	741.70	1.85	1.03	1.21
$Fe_{0.25}Co_{0.75}Sb_{2.96}Se_{0.04}$	9.0509	90°	741.43	1.65	2.34	2.09

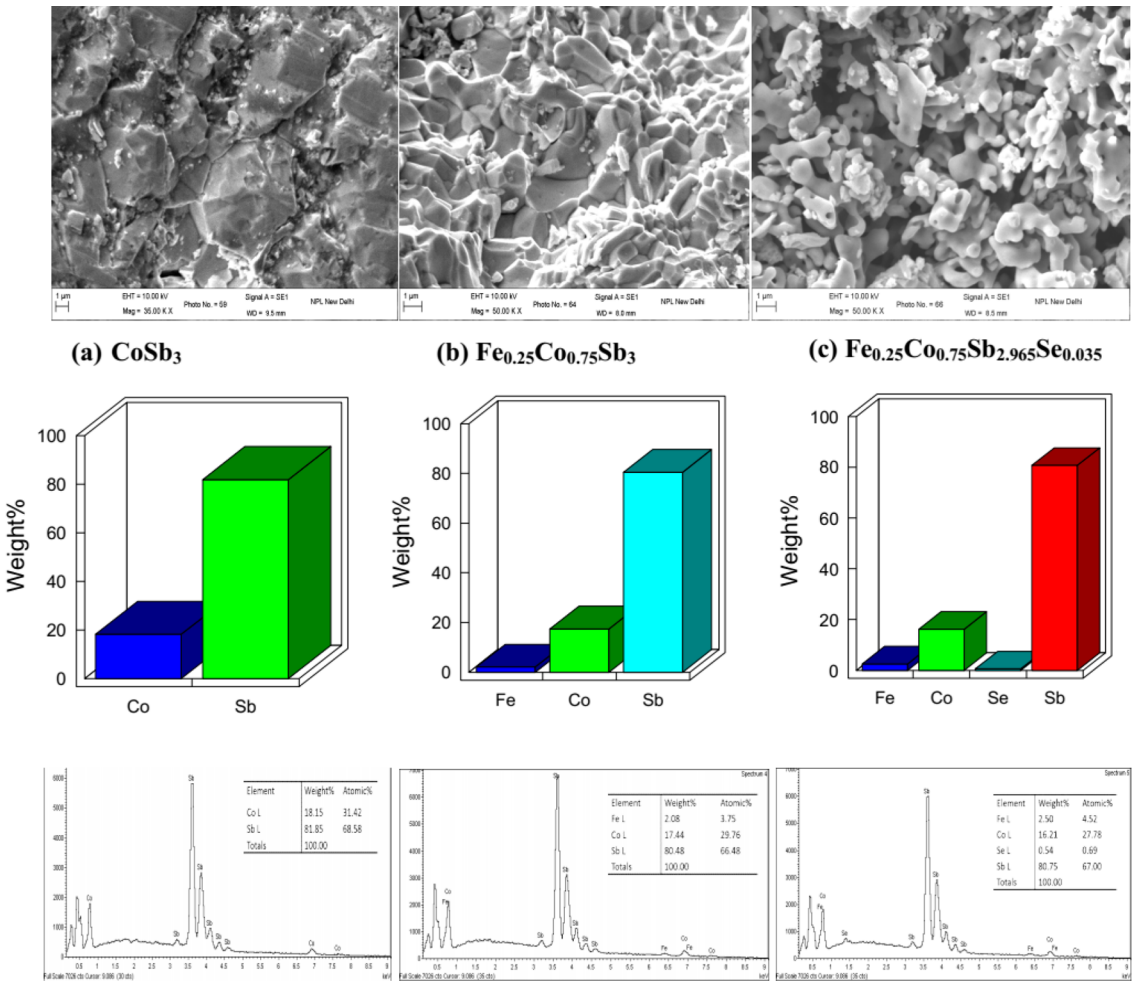

Figure 2. SEM images with corresponding quantitative elemental analysis and EDS spectrum of (a) $CoSb_3$, (b) $Fe_{0.25}Co_{0.75}Sb_3$, and (c) $Fe_{0.25}Co_{0.75}Sb_{2.965}Se_{0.035}$.

estimated using energy-dispersive X-ray spectroscopy (EDS). The Rietveld refinement was performed using the FullProf program.

The thermal diffusivity was measured using a Laser Flash analyzer (LFA, Linseis, 1023) on a polished disc sample of diameter 12.7 mm and thickness 2.5 mm, and the specific heat was measured employing a differential scanning calorimeter (DSC-Netzsch, 404 F3). The electrical conductivity and Seebeck coefficient were measured simultaneously over the range of the temperature of interest using a four-probe technique (Ulvac, ZEM 3), and the carrier concentration and mobility were measured using a Hall measurement system (HEMS, Nanomagnetics). All the synthesized samples exhibited a density >95% of the theoretical density, which was measured using the Archimedes principle. The accuracies in thermal and electronic transport measurements were the following: ∼±6% for thermal diffusivity, ∼±7% for electrical conductivity, ∼±7% for the Seebeck coefficient, and ∼±5% for specific heat. The reference materials used for the thermal diffusivity, Seebeck coefficient, and the specific heat measurements are inconel, constantan, and sapphire, respectively.

COMPUTATIONAL DETAILS

First-principles theoretical DFT-based calculations of the band structure and density of states (DOS) were performed using the all-electron full-potential linearized augmented plane wave (FP-LAPW) method as implemented in the WIEN2K code.[28] The $CoSb_3$ crystallizes in the $Im\bar{3}$ structure (space group no. 204), and the lattice constants and the atomic positions were taken from ref 16. Using supercells, the theoretical calculations were performed for $Co_3Fe_1Sb_{12}$, $Co_3Fe_1Sb_{11}Se_1$, and $Co_6Fe_2Sb_{23}Se_1$ compositions in order to understand the effect of partial substitution of Co by Fe and Sb by Se on the band structure of $CoSb_3$. The self-consistent calculations were carried out with 170 k points in the irreducible Brillouin zone (IBZ). We have used RK_{max} to be 7.0 while G_{max} is taken to be 12.0 $(au)^{-1}$, and the DFT calculations were carried out with a self-consistent field tolerance of 10^{-4} Ry. The electronic exchange-correlation energy was treated by the generalized gradient approximation (GGA).[29] The total and the angular momentum

DOI: 10.1021/acsaem.8b01609
ACS Appl. Energy Mater. 2019, 2, 1067−1076

decomposition of the atoms projected DOS was calculated using the same mesh for self-consistency. The electrical transport properties were calculated employing the BoltzTraP code[30] using 4350 and 2920 k-points in IBZ using a constant scattering time approximation. All calculations were done without incorporating spin−orbit coupling (SOC) as no influence of SOC was observed on the transport properties.

RESULTS AND DISCUSSION

The XRD patterns of all the pristine $CoSb_3$ and different doped compositions of $Fe_{0.25}Co_{0.75}Sb_{3-x}Se_x$ (x = 0, 0.02, 0.03, 0.035, 0.04) are shown in Figure 1a. This figure suggests that all the XRD peaks were indexed to the $CoSb_3$ phase and no secondary phase was noticed. Again, to confirm the phase purity and to evaluate the lattice parameters we have executed Rietveld refinement of all these XRD data. The Rietveld refined XRD pattern of one of the samples as shown in Figure 1b established the phase purity of the samples. The Rietveld refined crystallographic parameters are listed in Table 1 which designates that all the synthesized samples crystallized in the cubic phase with space group $Im\bar{3}$ (no. 204). The lattice parameter was found to decrease linearly with increasing Se content, as shown in Figure 1c, which is consistent with Vegard's law, thereby signifying a complete incorporation of the Se dopant in the matrix.

The surface morphology and the compositional analysis of the pristine and typical doped $CoSb_3$ samples were carried out through scanning electron microscopy (SEM) and are shown in Figure 2. This figure suggests that a non uniform coarse-grained microstructure is observed in the case of pristine $CoSb_3$ and the grains are tightly packed; this confirms the formation of highly dense bulk samples. After doping with Fe, as shown in Figure 2b, the material exhibits a regular plane shaped close packed surface, but the grain size is non uniform. Further, Figure 2c shows the morphology of the Fe and Se co-doped sample, and it shows that the grain size is reduced after doping which is caused by the insertion of an external atom (dopant), as these dopants suppress the grain-growth in the alloy. The elemental quantity as shown in Figure 2 for typical synthesized pristine and doped $CoSb_3$ samples validates that the actual elemental composition is very close to the initial nominal composition.

The band structure along with the partial DOS of pristine and doped $CoSb_3$ is shown in Figure 3, and the band structure is consistent with that calculated previously for $CoSb_3$.[17] It is evident from Figure 3a that $CoSb_3$ is a direct narrow band gap semiconductor with band gap ∼ 0.14 eV, which is in good agreement with earlier reports.[31−34]

This figure further suggests that, for the atom projected DOS, the Co atom has the maximum contribution and thus the features near the Fermi level are governed by the Co atom. However, after doping with Fe, the Fermi energy level shifts toward the valence band (Figure 3b) and thereby the material exhibits a p-type semiconducting behavior. Additionally, after Fe doping the charge transfer from the Fe to Co atom is clearly apparent in the electronic structure, which is expected to alter the electrical transport properties. Figure 3c also suggests that, after subsequent doping with Se on the Sb-site, although the band gap is reduced ∼ 0.06 eV, the behavior of the bands does not change significantly, except that the slopes of the bands become steeper, which is indicative of enhancement in the electrical transport properties. This has later been confirmed

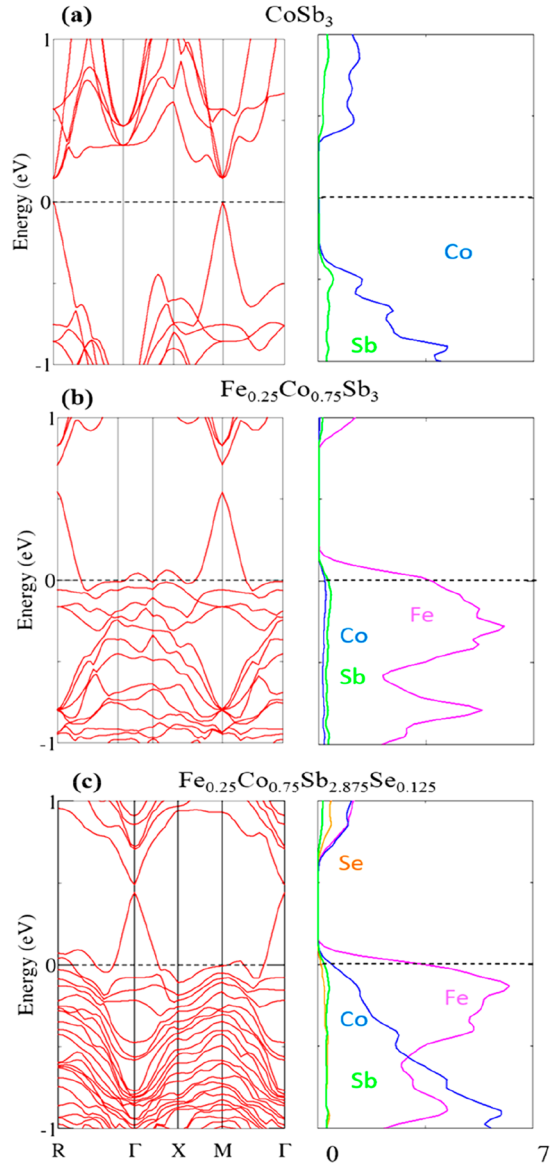

Figure 3. Band structure and partial density of states (DOS) of (a) $CoSb_3$, (b) $Fe_{0.25}Co_{0.75}Sb_3$, and (c) $Fe_{0.25}Co_{0.75}Sb_{2.875}Se_{0.125}$.

by the experimental results of the electrical transport properties.

The temperature dependence of the electrical transport properties of the synthesized pristine and (Fe, Se) co-doped $CoSb_3$ alloys for different compositions are depicted in Figure 4a,b. This figure suggest that while the pristine $CoSb_3$ exhibits a semiconducting behavior, the doped samples show a behavior akin to degenerate semiconductors, which is consistent with previous reports.[35] Furthermore, although the electrical resistivity (ρ) is found to decrease with Fe doping, it exhibits an increasing trend with Se doping. In order to understand the implication of co-doping in $CoSb_3$ on the electrical transport properties, the Hall measurements were performed at room temperature, and results are shown in Table 2. It is evident from this table that Fe doping at the Co-site in $CoSb_3$ introduces a large concentration of holes, as observed in a sample with composition $Fe_{0.25}Co_{0.75}Sb_3$, wherein the highest carrier (hole) concentration and moderate mobility led to a very high electrical conductivity (Figure 4a). Further, on Se co-doping in $Fe_{0.25}Co_{0.75}Sb_3$, due to electron

DOI: 10.1021/acsaem.8b01609
ACS Appl. Energy Mater. 2019, 2, 1067−1076

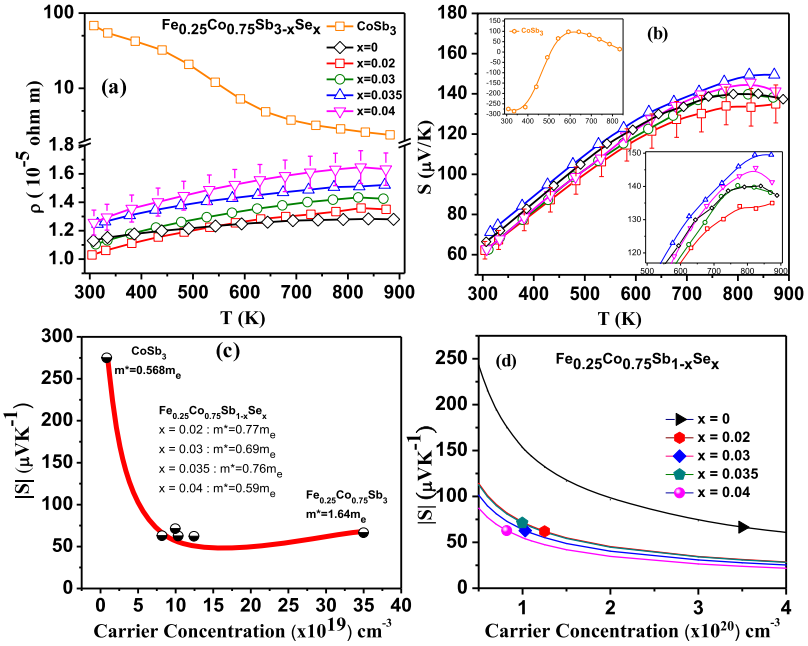

Figure 4. Temperature dependence of electrical transport properties of pristine $CoSb_3$ and $Fe_{0.25}Co_{0.75}Sb_{3-x}Se_x$ samples: (a) electrical resistivity, (b) Seebeck coefficient (S for pristine $CoSb_3$ in the first inset and magnified view of S in the second inset), (c) effective mass (m^*) derived from Seebeck coefficient and Hall Effect measurements, and (d) Pisarenko plot.

Table 2. Carrier Concentration, Mobility, and Other Electronic Transport Properties for Synthesized Pristine and Doped $CoSb_3$ at Room Temperature

composition	ρ (10^{-5} ohm m)	|S| (μV/K)	n (10^{19}/cm^3)	μ (cm^2/V s)	m^*
$CoSb_3$	68.1	275	0.84	370.56	$0.56m_e$
$Fe_{0.25}Co_{0.75}Sb_3$	1.13	66.50	35.63	17.40	$1.64m_e$
$Fe_{0.25}Co_{0.75}Sb_{2.98}Se_{0.02}$	1.03	62.2	12.46	53.41	$0.77m_e$
$Fe_{0.25}Co_{0.75}Sb_{2.97}Se_{0.03}$	1.10	62.6	10.34	53.65	$0.69m_e$
$Fe_{0.25}Co_{0.75}Sb_{2.965}Se_{0.035}$	1.24	71.2	9.97	54.07	$0.76m_e$
$Fe_{0.25}Co_{0.75}Sb_{2.96}Se_{0.04}$	1.26	62.8	8.20	55.65	$0.59m_e$

contribution by Se dopant on the Sb-site, the majority carrier (holes) concentration decreases, resulting in a lowering of the carrier effective mass and a corresponding increase in the carrier mobility.

In order to investigate the magnetic effect of Fe/Se doping, we have also performed the room temperature magnetic measurement using a vibrating sample magnetometer (Lakeshore-VSM 7410) up to a maximum applied field of 2 T, and the results are presented in Supporting Information (Figure S5). Although pristine $CoSb_3$ has a diamagnetic semiconducting nature,[36] it is clear from Figure S5 that after Fe doping magnetic behavior of all the samples changes to ferromagnetic and Se doping enhances the magnetization. Further, this magnetization increases with an increase in the Se doping, and it may contribute to the transport properties in a systematic manner although in a very limited way.[37]

The temperature-dependent Seebeck coefficients (S) of the pristine and doped $CoSb_3$ samples are shown in Figure 4b and clearly underline that all the doped $CoSb_3$ samples exhibit a positive Seebeck coefficient. Further, we observed that the Seebeck coefficient linearly increases with the temperature and attains a maximum value of ~150 μV/K at 870 K for the optimized sample composition $Fe_{0.25}Co_{0.75}Sb_{2.965}Se_{0.035}$. This measured Seebeck coefficient is higher than that reported earlier for the p-type $CoSb_3$/graphene nanocomposite at 850 K[24] and close to that reported for Yb-filled $CoSb_3$.[38] The temperature dependence of the Seebeck coefficient of pristine $CoSb_3$, as shown in the inset of Figure 4b, exhibits a bipolar conduction due to the thermal excitation of minority charge carriers, which is in line with the observations reported earlier.[16−18] It may be noted that the bipolar conduction in the $CoSb_3$ alloy is known to be detrimental for the enhancement of ZT. However, this unfavorable TE nature of $CoSb_3$ could be utilized for realization of n- or p-type TE material. In the present work it has been exploited by the substitution of Fe on the Co-site, thereby resulting in p-type conduction, over the entire temperature range of measurement. Furthermore, the substitutional co-doping by Se on the Sb-site in $CoSb_3$ leads to optimization of the carrier concentrations and to an increase in the Seebeck coefficient.

In the degenerate limit, under the assumptions of a single parabolic band model and an energy-independent relaxation time with standard carrier acoustic phonon scattering as the dominant scattering mechanism, the relationship among S, m^*, and n can be described as[2]

$$S = \left(\frac{8\pi^2 k_B^2}{3eh^2}\right) m^* T \left(\frac{\pi}{3n}\right)^{2/3}$$

where k_B is the Boltzmann constant, h is Planck's constant, e is the carrier charge, n is the carrier concentration. The estimated

DOI: 10.1021/acsaem.8b01609
ACS Appl. Energy Mater. 2019, 2, 1067−1076

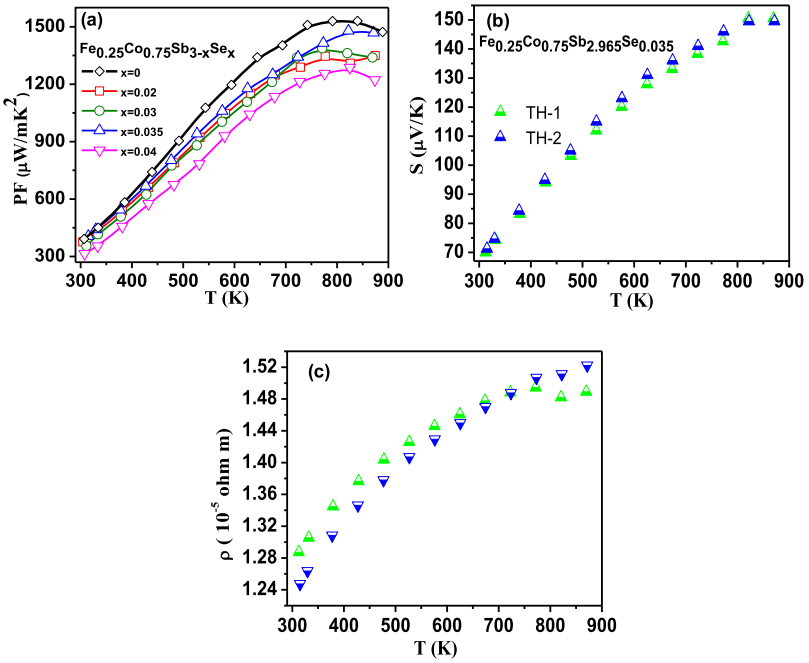

Figure 5. Temperature-dependent (a) power factor for all the doped samples and repeatability data, (b) Seebeck coefficient, and (c) electrical resistivity for optimized $Fe_{0.25}Co_{0.75}Sb_{2.965}Se_{0.035}$ sample.

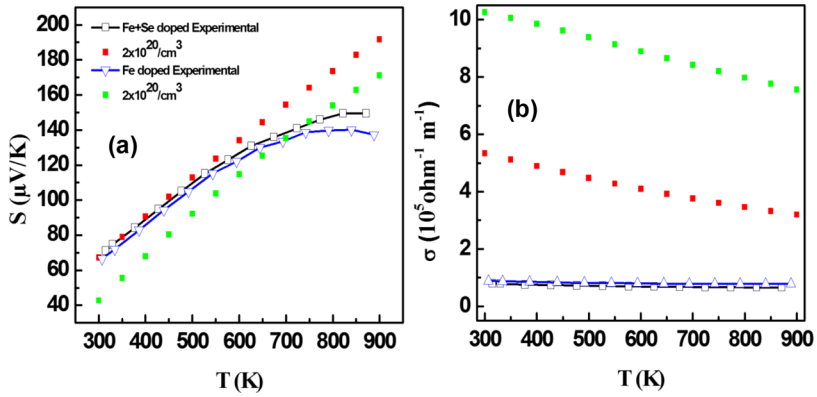

Figure 6. Comparison of experimentally measured and theoretically calculated (a) Seebeck coefficient and (b) electrical conductivity.

carrier effective mass (m^*) for different compositions is shown in Figure 4c.

It is evident from the figure that pristine $CoSb_3$ exhibits $m^* = 0.568m_e$, which explains the very high observed mobility (μ) observed by Hall measurements. On Fe doping in $CoSb_3$, the m^* increases to $1.64m_e$, which may be substantially attributed to band non-parabolicity observed previously for heavily doped $CoSb_3$,[17] thereby resulting in a decrease in the mobility. On Se doping, m^* was found to be largely decreased with an invariable or marginally decreased Seebeck, as observed in Figure 4b. The variation in Fe and Se co-doped $CoSb_3$ samples suggests that the m^* changes in accordance with the non-parabolic type dispersion (as linear or Kane bands) and can be defined by energy-dependent effective mass derived from the electron momentum. The estimated m^* is similar to that reported earlier for $CoSb_3$-based alloys with similar compositions.[2,17,39]

To further elucidate the observed phenomenon, a Pisarenko plot for doped composition is shown in Figure 4d, which displays a nonmonotonic variation with the Se doping content, suggesting band non-parabolicity, a behavior common in narrow band gap semiconductors, with a nearly linear dispersion.

Figure 5a shows the temperature dependence of the power factor (PF), $S^2\sigma$, of all the doped samples, which shows an increasing trend with respect to temperature. Also, it is to be noted that the sample $Fe_{0.25}Co_{0.75}Sb_3$ has the highest power factor among all the doped samples ($\sim 1.47 \times 10^3$ μW/mK^2 at 870 K) due to its higher electrical conductivity, although this value is comparable to the power factor of the $Fe_{0.25}Co_{0.75}Sb_{2.965}Se_{0.035}$ sample ($\sim 1.46 \times 10^3$ μW/mK^2 at 870 K). Figure 5b,c represents the repeatability data for the temperature-dependent Seebeck coefficient and the electrical resistivity for the sample $Fe_{0.25}Co_{0.75}Sb_{2.965}Se_{0.035}$, which contains data for two thermal cycles named TH-1 and TH-2. As is evident, both the plots are almost parallel to each other; hence, the thermal and chemical stability of the material is persistent.

Furthermore, using the Goldsmid–Sharp band gap equation,[40] the thermal band gap was estimated and was found to be in the range 0.21–0.26 eV for Fe and Se co-doped samples and 0.505 eV for the pristine $CoSb_3$, which is in agreement with the values reported previously for similar skutterudite

DOI: 10.1021/acsaem.8b01609
ACS Appl. Energy Mater. 2019, 2, 1067–1076

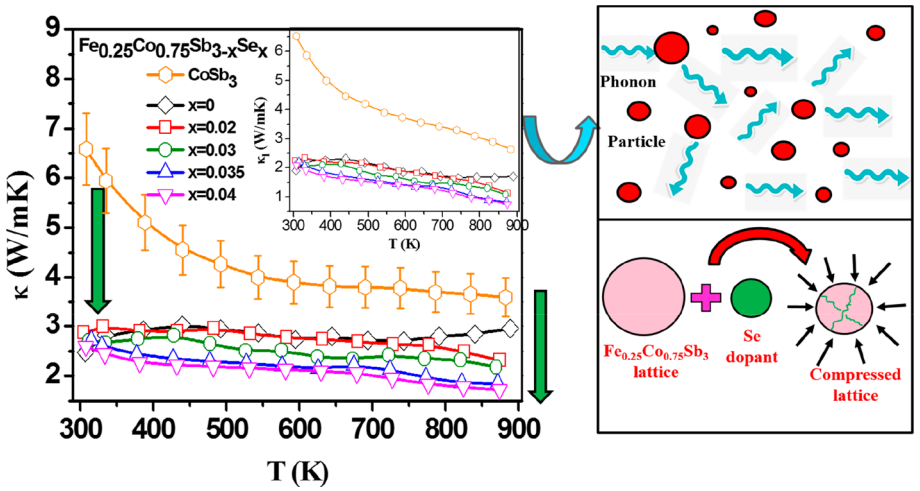

Figure 7. Temperature dependence of the total thermal conductivity with lattice thermal conductivity (inset) along with the phonon scattering and mass fluctuation mechanism.

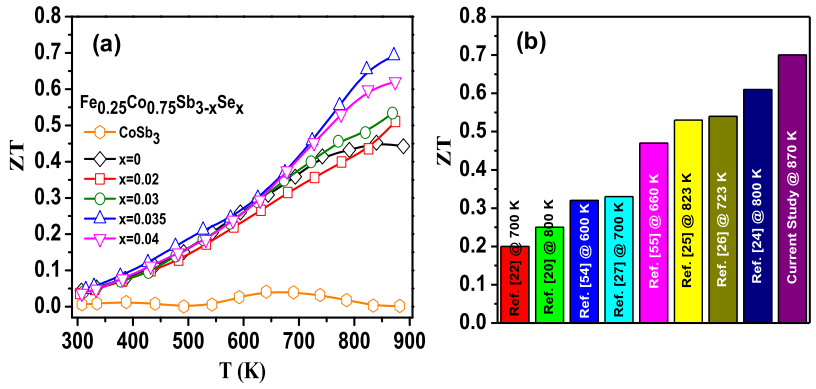

Figure 8. (a) Temperature dependence of ZT for pristine $CoSb_3$ and $Fe_{0.25}Co_{0.75}Sb_{3-x}Se_x$ samples and (b) comparison of ZT values with those reported in the literature for p-type unfilled $CoSb_3$-based skutterudites.

compositions.[41] The experimentally observed electrical transport properties as a result of co-doping of Fe and Se in $CoSb_3$ are in broad agreement with those predicted theoretically from DFT-based band structure calculations as discussed earlier (Figure 3).

For a better understanding we have extended our DFT calculations for electrical transport properties using Boltztrap code. The temperature variation of the theoretically calculated transport properties of Fe and Se co-doped $CoSb_3$ samples along with the comparison of experimentally observed transport properties is shown in Figure 6, which shows that at an optimized carrier concentration $\sim 2 \times 10^{20}/cm^3$ the experimentally observed Seebeck coefficient is in reasonably good agreement with its theoretically predicted values (Figure 6a), especially at lower temperatures. It may be noted from Figure 6b that the experimental and theoretical behaviors of the electrical conductivity are qualitatively similar although quantitatively their magnitudes are different, which may be due to the limitations of the constant relaxation time approximation made in the theoretical calculations. Also, the theoretical transport properties for a wide range of carrier concentration are given in Supporting Information (Section 1).

The thermal conductivity is calculated as a product of specific heat, thermal diffusivity, and density as shown in the Supporting Information (Section 3). It has a contribution from both the lattice and the electronic part; therefore, their individual contributions have been estimated using the Wiedemann–Franz law $\kappa_e = L\sigma T$, where L is the Seebeck-coefficient-dependent Lorentz number, which has been calculated employing the equation[42]

$$L = 1.5 + \exp\left[\frac{-|S|}{116}\right]$$

Here, S is the Seebeck coefficient in $\mu V/K$. The temperature-dependent plot of the Lorentz number for pristine and doped $CoSb_3$ is shown in Supporting Information (Section 2). Figure 7 shows the variation of thermal conductivity with temperature along with its lattice counterpart (inset) for pristine as well as doped $CoSb_3$ samples. It is apparent from this figure that the thermal conductivity of the $Fe_{0.25}Co_{0.75}Sb_3$ sample is ~ 3 $Wm^{-1}K^{-1}$ at 870 K, which gets substantially reduced to ~ 1.85 $Wm^{-1}K^{-1}$ after Se doping (sample composition), which is much less than the thermal conductivity of pristine $CoSb_3$ at 870 K (~ 3.6 Wm^{-1} K^{-1} as visible in Figure 7) and close to that reported for filled skutterudites.[10,43−46] It is also evident from the inset of Figure 7 that the lattice thermal conductivity contributes significantly to the total thermal conductivity, which indicates the dominance of the phonon scattering mechanism in the reduction of the thermal conductivity. Such a drastic reduction in thermal conductivity may be ascribed to enhanced scattering of heat carrying phonons due to the substitutional defects caused by Se doping, which can induce

DOI: 10.1021/acsaem.8b01609
ACS Appl. Energy Mater. 2019, 2, 1067−1076

mass fluctuations owing to a large difference in the ionic size and atomic mass of Se and Sb.[47] Also, this phonon scattering due to substitutional defects is dominant at high temperature, and hence, a greater reduction in thermal conductivity at high temperature occurs. Further, the SEM image of the Se doped sample (Figure 2c) also indicates the lowering of grain size which is also responsible for reduction in thermal conductivity. Also, with deliberate doping the anharmonicity can be generated in phonon dispersion,[48] which is the measure of deviation from ideal harmonic behavior and can boost strong phonon−phonon scattering resulting in reduced lattice thermal conductivity.[49] Some reports are also available on anharmonicity in skutterudites (mainly filled skutterudites).[50−53]

Figure 8a shows the temperature dependence of ZT for the pristine and doped composition of $CoSb_3$, which suggests that an enhanced ZT ∼ 0.7 at 870 K has been realized for the optimized skutterudite composition of $Fe_{0.25}Co_{0.75}Sb_{2.965}Se_{0.035}$, which is the highest reported thus far for unfilled p-type $CoSb_3$-skuttrudites and is higher than its pristine counterpart (0.002 at 870 K) by 2 orders of magnitude. This enhancement in ZT is attributed to optimized carrier concentration after co-doping in $CoSb_3$ as well as reduced thermal conductivity due to enhanced phonon scattering induced by point defects created through substitutional doping. Also, it is evident from Figure 8a that there is a large enhancement in ZT at higher temperature, which is due to dominant phonon scattering at high temperature. Thus, reduction in thermal conductivity is mainly responsible for the enhancement in ZT at high temperature (post-doping).

Figure 8b shows a relative comparison of the reported ZT values for p-type $CoSb_3$-based skutterudites,[20,22,24−27,54,55] which suggests that this value of ZT realized in the present study is far higher than those previously reported for p-type $CoSb_3$ unfilled skutterudites.[20,22,24−27,54,55] To govern the usefulness of the material, the average ZT has also been calculated and the comparison chart with previous reports is shown in Supporting Information (Section 4).

CONCLUSIONS

In this study, a state-of-the-art ZT ∼ 0.7 at 870 K was realized in an optimized skutterudite composition of $Fe_{0.25}Co_{0.75}Sb_{2.965}Se_{0.035}$, which is a rare-earth-free $CoSb_3$-based p-type thermoelectric material, synthesized using a facile process of arc-melting and spark plasma sintering, which is both fast and scalable. The experimental results suggest that the optimized partial substitutional doping of Fe at the Co-site and Se at the Sb-site in $CoSb_3$ results in a favorable tuning of the electrical and thermal transport properties leading to an enhanced ZT, which is higher by 2 orders of magnitude than that of its synthesized pristine counterpart and also nearly 4 times that reported earlier for pristine $CoSb_3$. The theoretically estimated transport properties of pristine and doped $CoSb_3$, calculated employing the first-principles-based density functional theory and Boltzmann transport equations, were found to be in good qualitative agreement with those measured experimentally.

ASSOCIATED CONTENT

Supporting Information

The Supporting Information is available free of charge on the ACS Publications website at DOI: 10.1021/acsaem.8b01609.

Theoretically calculated temperature-dependent electrical transport properties, temperature-dependent Lorentz number, thermal diffusivity, and specific heat; comparison of average ZT with previous reports; and room temperature magnetic hysteresis plots for all the doped $CoSb_3$ samples (PDF)

AUTHOR INFORMATION

Corresponding Authors

*E-mail: bhasker@nplindia.org.

*E-mail: adhar@nplindia.org. Phone: +91-11-45609456. Fax: +91-11-45609310.

ORCID

Sivaiah Bathula: 0000-0001-6093-6351

Nagendra S. Chauhan: 0000-0003-2579-6642

Ajay Dhar: 0000-0001-7494-0378

Notes

The authors declare no competing financial interest.

ACKNOWLEDGMENTS

The authors sincerely acknowledge the Board of Research in Nuclear Sciences (Sanction No: 37(3)/14/22/2016-BRNS/37055), India, for the financial support. R.B. would like to acknowledge the financial support from DST-India as an INSPIRE-Junior Research Fellowship. The technical support rendered by Mr. Radhey Shyam and Mr. Naval Kishor Upadhyay is also gratefully acknowledged. The authors also acknowledge Dr. Alexandra Zevalkink, Michigan State University, for the fruitful discussions and suggestions. S.A. would like to acknowledge the use of the High-Performance Computing (HPC) facilities at the Physics Department of the Indian Institute of Technology in Kanpur (IITK), Intra-University Accelerator Centre (IUAC) in New Delhi, Institute of Mathematical Sciences (IMSC) in Chennai, and Council of Scientific and Industrial Research Fourth Paradigm Institute (CSIR-4PI) at Bengaluru and University of Hyderabad in Hyderabad.

REFERENCES

(1) Orr, B.; Akbarzadeh, A.; Mochizuki, M.; Singh, R. A Review of Car Waste Heat Recovery Systems Utilising Thermoelectric Generators and Heat Pipes. *Appl. Therm. Eng.* **2016**, *101*, 490−495.

(2) Chauhan, N. S.; Bathula, S.; Vishwakarma, A.; Bhardwaj, R.; Gahtori, B.; Kumar, A.; Dhar, A. Vanadium-Doping-Induced Resonant Energy Levels for the Enhancement of Thermoelectric Performance in Hf-Free ZrNiSn Half-Heusler Alloys. *ACS Appl. Energy Mater.* **2018**, *1*, 757−764.

(3) Chauhan, N. S.; Bathula, S.; Vishwakarma, A.; Bhardwaj, R.; Johari, K. K.; Gahtori, B.; Saravanan, M.; Dhar, A. Compositional Tuning of ZrNiSn Half-Heusler Alloys: Thermoelectric Characteristics and Performance Analysis. *J. Phys. Chem. Solids* **2018**, *123*, 105−112.

(4) Chauhan, N. S.; Bathula, S.; Vishwakarma, A.; Bhardwaj, R.; Kumar Johari, K.; Gahtori, B.; Dhar, A. Facile Fabrication of P- and n-Type Half-Heusler Alloys with Enhanced Thermoelectric Performance and Low Specific Contact Resistance Employing Spark Plasma Sintering. *Mater. Lett.* **2018**, *228*, 250−253.

(5) Upadhyay, N. K.; Kumaraswamidhas, L. A.; Gahtori, B.; Bathula, S.; Muthiah, S.; Shyam, R.; Chauhan, N. S.; Bhardwaj, R.; Dhar, A. Enhancement in Thermoelectric Performance of Bulk CrSi2 Dispersed with Nanostructured SiGe Nanoinclusions. *J. Alloys Compd.* **2018**, *765*, 412−417.

(6) Goldsmid, H. J. Bismuth Telluride and Its Alloys as Materials for Thermoelectric Generation. *Materials* **2014**, *7*, 2577−2592.

(7) Pei, Y.; Shi, X.; Lalonde, A.; Wang, H.; Chen, L.; Snyder, G. J. Convergence of Electronic Bands for High Performance Bulk Thermoelectrics. *Nature* **2011**, *473*, 66−69.
(8) Hsu, K. F.; Loo, S.; Guo, F.; Chen, W.; Dyck, J. S.; Uher, C.; Hogan, T.; Polychroniadis, E.; Kanatzidis, M. G. Cubic $AgPb_mSbTe_{2+m}$: Bulk Thermoelectric Materials with High Figure of Merit. *Science* **2004**, *303*, 818−821.
(9) Kim, J.; Ohishi, Y.; Muta, H.; Kurosaki, K. Enhancement of Thermoelectric Properties of p -Type Single-Filled Skutterudites $Ce_xFe_yCo_{4-y}Sb_{12}$ by Tuning the Ce and Fe Content. *AIP Adv.* **2018**, *8*, 105104.
(10) Rull-Bravo, M.; Moure, A.; Fernández, J. F.; Martín-González, M. Skutterudites as Thermoelectric Materials: Revisited. *RSC Adv.* **2015**, *5*, 41653−41667.
(11) Oftedal, I. XXXIII. Die Kristallstruktur von Skutterudit Und Speiskobalt-Chloanthit. *Z. Kristallogr. - Cryst. Mater.* **1928**, *66*, 517−546.
(12) Carlini, R.; Fanciulli, C.; Boulet, P.; Record, M. Skutterudites for Thermoelectric Applications: Properties, Synthesis and Modelling. 2017.
(13) Yang, J.; Zhang, W.; Bai, S. Q.; Mei, Z.; Chen, L. D. Dual-Frequency Resonant Phonon Scattering in Bax Ry Co_4Sb_{12} (R = La, Ce, and Sr). *Appl. Phys. Lett.* **2007**, *90*, 192111.
(14) Rogl, G.; Aabdin, Z.; Schafler, E.; Horky, J.; Setman, D.; Zehetbauer, M.; Kriegisch, M.; Eibl, O.; Grytsiv, A.; Bauer, E.; et al. Effect of HPT Processing on the Structure, Thermoelectric and Mechanical Properties of $Sr_{0.07}Ba_{0.07}Yb_{0.07}Co_4Sb_{12}$. *J. Alloys Compd.* **2012**, *537*, 183−189.
(15) Rogl, G.; Grytsiv, A.; Rogl, P.; Peranio, N.; Bauer, E.; Zehetbauer, M.; Eibl, O. N-Type Skutterudites $(R,Ba,Yb)_YCo_4Sb_{12}$ (R = Sr, La, Mm, DD, SrMm, SrDD) Approaching ZT ≈ 2.0. *Acta Mater.* **2014**, *63*, 30−43.
(16) Kawaharada, Y.; Kurosaki, K.; Uno, M.; Yamanaka, S. Thermoelectric Properties of $CoSb_3$. *J. Alloys Compd.* **2001**, *315*, 193−197.
(17) Tang, Y.; Gibbs, Z. M.; Agapito, L. A.; Li, G.; Kim, H. S.; Nardelli, M. B.; Curtarolo, S.; Snyder, G. J. Convergence of Multi-Valley Bands as the Electronic Origin of High Thermoelectric Performance in $CoSb_3$ Skutterudites. *Nat. Mater.* **2015**, *14*, 1223−1228.
(18) Liu, W. S.; Zhang, B. P.; Li, J. F.; Zhao, L. D. Effects of Sb Compensation on Microstructure, Thermoelectric Properties and Point Defect of $CoSb_3$ Compound. *J. Phys. D: Appl. Phys.* **2007**, *40*, 6784−6790.
(19) Toprak, M. S.; Stiewe, C.; Platzek, D.; Williams, S.; Bertini, L.; Müller, E.; Gatti, C.; Zhang, Y.; Rowe, M.; Muhammed, M. The Impact of Nanostructuring on the Thermal Conductivity of Thermoelectric $CoSb_3$. *Adv. Funct. Mater.* **2004**, *14*, 1189−1196.
(20) Tafti, M. Y.; Saleemi, M.; Toprak, M. S.; Johnsson, M.; Jacquot, A.; Jägle, M.; Muhammed, M. Fabrication and Characterization of Nanostructured Thermoelectric $Fe_xCo_{1-x}Sb_3$. *Open Chemistry* **2015**, *13*. DOI: 10.1515/chem-2015-0074
(21) Alboni, P. N.; Ji, X.; He, J.; Gothard, N.; Tritt, T. M. Thermoelectric Properties of $La_{0.9}CoFe_3Sb_{12}$-$CoSb_3$ Skutterudite Nanocomposites. *J. Appl. Phys.* **2008**, *103*, 113707.
(22) Kim, I.-H.; Ur, S.-C. Electronic Transport Properties of Fe-doped $CoSb_3$ Prepared by Encapsulated Induction Melting. *Mater. Lett.* **2007**, *61*, 2446−2450.
(23) Wojciechowski, K.; Toboła, J.; Leszczyński, J. Thermoelectric Properties and Electronic Structure of $CoSb_3$ Doped with Se and Te. *J. Alloys Compd.* **2003**, *361*, 19−27.
(24) Feng, B.; Xie, J.; Cao, G.; Zhu, T.; Zhao, X. Enhanced Thermoelectric Properties of p-type CoSb 3/Graphene Nano-composite. *J. Mater. Chem. A* **2013**, *1*, 13111−13119.
(25) Liu, Y.; Li, X.; Zhang, Q.; Chen, C.; Li, J.; Zhang, L.; Yu, D.; Tian, Y.; Xu, B. High Pressure Synthesis of P-Type Fe-Substituted $CoSb_3$ Skutterudites. *J. Mater. Sci.: Mater. Electron.* **2016**, *27*, 6433−6437.
(26) Park, K.-H.; Kim, I.-H. Thermoelectric Properties of $Co_{4-x}Mn_xSb_{12-y}$ Sn y Skutterudites. *Electron. Mater. Lett.* **2011**, *7*, 39.
(27) Ioannidou, A. A.; Rull, M.; Martin-Gonzalez, M.; Moure, A.; Jacquot, A.; Niarchos, D. Microwave Synthesis and Characterization of the Series Co1-XFexSb3 high Temperature Thermoelectric Materials. *J. Electron. Mater.* **2014**, *43*, 2637−2643.
(28) Blaha, P.; Schwarz, K.; Madsen, G.; Kvasnicka, D.; Luitz, J. wien2k. An Augmented Plane Wave+ Local Orbitals Program for Calculating Crystal Properties. 2001.
(29) Perdew, J. P.; Burke, K.; Ernzerhof, M. Generalized Gradient Approximation Made Simple. *Phys. Rev. Lett.* **1996**, *77*, 3865−3868.
(30) Madsen, G. K. H.; Singh, D. J. BoltzTraP. A Code for Calculating Band-Structure Dependent Quantities. *Comput. Phys. Commun.* **2006**, *175*, 67−71.
(31) Chaput, L.; Pécheur, P.; Tobola, J.; Scherrer, H. Transport in Doped Skutterudites: Ab Initio Electronic Structure Calculations. *Phys. Rev. B: Condens. Matter Mater. Phys.* **2005**, *72*, No. 085126.
(32) Singh, D. J.; Pickett, W. E. Skutterudite Antimonides: Quasilinear Bands and Unusual Transport. *Phys. Rev. B: Condens. Matter Mater. Phys.* **1994**, *50*, 11235−11238.
(33) Sofo, J.; Mahan, G. Electronic Structure of A Narrow-Band-Gap Semiconductor. *Phys. Rev. B: Condens. Matter Mater. Phys.* **1998**, *58*, 15620−15623.
(34) Kurmaev, E. Z.; Moewes, A.; Shein, I. R.; Finkelstein, L. D.; Ivanovskii, A. L.; Anno, H. Electronic Structure and Thermoelectric Properties of Skutterudite Compounds. *J. Phys.: Condens. Matter* **2004**, *16*, 979−987.
(35) Mallik, R.; Anbalagan, R.; Rogl, G.; Royanian, E.; Heinrich, P.; Bauer, E.; Rogl, P.; Suwas, S. Thermoelectric Properties of $Fe_{0.2}Co_{3.8}Sb_{12-x}Te_x$ Skutterudites. *Acta Mater.* **2013**, *61*, 6698−6711.
(36) Yang, J.; Meisner, G. P.; Morelli, D. T.; Uher, C. Iron Valence in Skutterudites: Transport and Magnetic Properties of. *Phys. Rev. B: Condens. Matter Mater. Phys.* **2000**, *63*, No. 014410.
(37) Acharya, S.; Anwar, S.; Mori, T.; Soni, A. Coupling of Charge Carriers with Magnetic Entropy for Power Factor Enhancement in Mn Doped $Sn_{1.03}$ Te for Thermoelectric Applications. *J. Mater. Chem. C* **2018**, *6*, 6489−6493.
(38) Zhou, C.; Morelli, D.; Zhou, X.; Wang, G.; Uher, C. Thermoelectric Properties of P-type Yb-Filled Skutterudite YbxFey-Co4-ySb12. *Intermetallics* **2011**, *19*, 1390−1393.
(39) Su, X.; Li, H.; Yan, Y.; Chi, H.; Tang, X.; Zhang, Q.; Uher, C. The role of Ga in $Ba_{0.30}Ga_xCo_4Sb_{12+x}$ Filled Skutterudites. *J. Mater. Chem.* **2012**, *22*, 15628−15634.
(40) Goldsmid, H. J.; Sharp, J. W. Estimation of the Thermal Band Gap of a Semiconductor from Seebeck Measurements. *J. Electron. Mater.* **1999**, *28*, 869−872.
(41) Mandrus, D.; Migliori, A.; Darling, T. W.; Hundley, M. F.; Peterson, E. J.; Thompson, J. D. Electronic Transport in Lightly Doped $CoSb_3$. *Phys. Rev. B: Condens. Matter Mater. Phys.* **1995**, *52*, 4926−4931.
(42) Kim, H.-S.; Gibbs, Z. M.; Tang, Y.; Wang, H.; Snyder, G. J. Characterization of Lorenz Number with Seebeck Coefficient Measurement. *APL Mater.* **2015**, *3*, 041506.
(43) Prado-Gonjal, J.; Vaqueiro, P.; Nuttall, C.; Potter, R.; Powell, A. V. Enhancing the Thermoelectric Properties of Single and Double Filled P-Type Skutterudites Synthesized by an up-Scaled Ball-Milling Process. *J. Alloys Compd.* **2017**, *695*, 3598−3604.
(44) Sales; Mandrus; Williams. Filled Skutterudite Antimonides: A New Class of Thermoelectric Materials. *Science* **1996**, *272* (5266), 1325−1328.
(45) Zhang, L.; Grytsiv, A.; Rogl, P.; Bauer, E.; Zehetbauer, M. High Thermoelectric Performance of Triple-Filled n-Type Skutterudites $(Sr,Ba,Yb)YCo_4Sb_{12}$. *J. Phys. D: Appl. Phys.* **2009**, *42*, 225405.
(46) Shi, X.; Kong, H.; Li, C.-P.; Uher, C.; Yang, J.; Salvador, J.; Wang, H.; Chen, L.; Zhang, W. Low Thermal Conductivity and High Thermoelectric Figure of Merit in n-type $Ba_xYb_yCo_4Sb_{12}$ Double-Filled Skutterudites. *Appl. Phys. Lett.* **2008**, *92*, 182101.

DOI: 10.1021/acsaem.8b01609
ACS Appl. Energy Mater. 2019, 2, 1067−1076

(47) He, J.; Kanatzidis, M. G.; Dravid, V. P. High Performance Bulk Thermoelectrics via a Panoscopic Approach. *Mater. Today* **2013**, *16*, 166−176.
(48) Acharya, S.; Pandey, J.; Soni, A. Soft Phonon Modes Driven Reduced Thermal Conductivity in Self-Compensated Sn1.03Te with Mn Doping. *Appl. Phys. Lett.* **2016**, *109*, 133904.
(49) Jana, M. K.; Biswas, K. Crystalline Solids with Intrinsically Low Lattice Thermal Conductivity for Thermoelectric Energy Conversion. *ACS Energy Lett.* **2018**, *3*, 1315−1324.
(50) Meng, X.; Liu, Z.; Cui, B.; Qin, D.; Geng, H.; Cai, W.; Fu, L.; He, J.; Ren, Z.; Sui, J. Grain Boundary Engineering for Achieving High Thermoelectric Performance in N-Type Skutterudites. *Adv. Energy Mater.* **2017**, *7*, 1602582.
(51) Tsutsui, S.; Kobayashi, H.; Sutter, J. P.; Uchiyama, H.; Baron, A. Q. R.; Yoda, Y.; Kikuchi, D.; Sugawara, H.; Sekine, C.; Shirotani, I.; et al. Investigation of the Anharmonic Guest Modes in Filled Skutterudites Using Inelastic X-Ray Scattering Techniques. *J. Phys. Soc. Jpn.* **2008**, *77*, 257−259.
(52) Feldman, J. L.; Singh, D. J.; Kendziora, C.; Mandrus, D.; Sales, B. C. Lattice Dynamics of Filled Skutterudites: $La(Fe,Co)_4Sb_{12}$. *Phys. Rev. B: Condens. Matter Mater. Phys.* **2003**, *68*, 94301−94311.
(53) Sergueev, I.; Glazyrin, K.; Kantor, I.; McGuire, M. A.; Chumakov, A. I.; Klobes, B.; Sales, B. C.; Hermann, R. P. Quenching Rattling Modes in Skutterudites with Pressure. *Phys. Rev. B: Condens. Matter Mater. Phys.* **2015**, *91*, 224304.
(54) Ur, S. C.; Kwon, J. C.; Kim, I. H. Thermoelectric Properties of Fe-Doped CoSb3 Prepared by Mechanical Alloying and Vacuum Hot Pressing. *J. Alloys Compd.* **2007**, *442* (1−2), 358−361.
(55) Wang, H.; Li, S.; Li, X.; Zhong, H. Microstructure and Thermoelectric Properties of Doped P-Type $CoSb_3$ under TGZM Effect. *J. Cryst. Growth* **2017**, *466*, 56−63.

DOI: 10.1021/acsaem.8b01609
ACS Appl. Energy Mater. 2019, 2, 1067−1076